Pergamon

Journal of Structural Geology, Vol. 20, No. 2/3, pp. 277 to 292, 1998

PII: S0191-8141(97)00084-9
0191-8141/98 $19.00 + 0.00

Seismic properties of highly strained marbles from the Splügenpass, central Alps

L. BURLINI

Centro di Studio per la Geodinamica Alpina e Quaternaria CNR, via Botticelli, 23, 20133 Milano, Italy

D. MARQUER and N. CHALLANDES

University of Neuchatel, Geological Institute, rue E. Argand, 11; CH2007 Neuchatel, Switzerland

S. MAZZOLA and N. ZANGARINI

Dipartimento di Scienze della Terra, University of Milan, via Mangiagalli, 34, 20133 Milano, Italy

(*Received* 28 *January* 1997; *accepted in revised form* 23 *September* 1997)

Abstract—Seismic reflection profiling across the Central Alps (NFP20) shows strong reflectors, some of which correspond to a Mesozoic marble zone which underlies the contact between the Tambo and Suretta nappes. By means of experimental velocity measurements at confining pressures up to 300 MPa on rock samples collected in the marble zone, we determined the seismic properties of these marbles and calculated their reflection coefficients, in order better to constrain the seismic interpretation.

The main findings are as follows:

a) Marbles exhibit V_p anisotropy up to 9%, with orthorhombic or transverse isotropic (tetragonal) symmetry due to the crystallographic preferred orientation of calcite.
b) Compressional waves, shear waves, and shear wave splitting are very sensitive to the type of fabric (presence or absence of an *r*-axes concentration).
c) Interfaces between marbles and amphibolites or orthogneisses could be good reflectors in normal incidence reflection. © 1998 Elsevier Science Ltd.

INTRODUCTION

The seismic studies conducted over the past years (NFP20, CROP-01) have helped to revolutionise our interpretation of the Central Alps. The geological interpretation of the geometry imaged by deep seismic profiling unfortunately is non-unique since it is very difficult to assign rock types to the structure observed. Many rock types can display similar velocities and other properties such as anisotropy, and fluid filled cracks and temperature variations affect the seismic velocity.

In the Central Alps, across Switzerland and N Italy, strong reflections at 2–10 km depth have been observed in the recent investigations by seismic reflection profiling (NFP-20 and CROP-01), and some of these reflectors were interpreted as contacts between nappes (Fig. 1), which are exposed on the surface (Pfiffner *et al.*, 1990a,b). In order better to constrain the interpretation of the

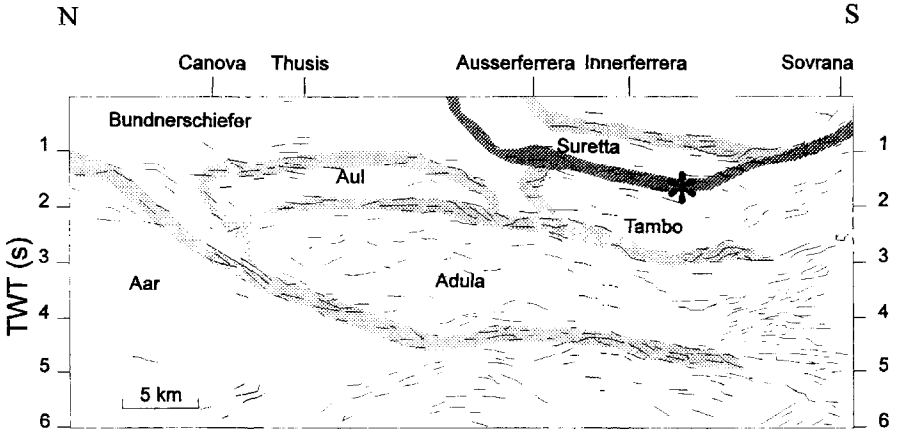

Fig. 1. Interpreted line drawing of the N–S NFP-20 near vertical reflection profile across the Central Alps located E of the Splügenpass (from Pfiffner *et al.*, 1990a redrawn). The shaded area has been interpreted by Pfiffner *et al.* (1990a,b) as the limits between nappes represented by the carbonate cover rocks. Note the intense reflectivity of these zones, separated by almost non-reflective lenses. These reflective horizons tend to anastomose. The darker shaded area may represent the Splügenzone, and the asterisk indicates the studied area.

nature of these reflectors, the seismic properties at pressures up to 300 MPa have been measured on several rock samples from the cover rocks pinched between the Tambo and Suretta nappes, which belong to the eastern Swiss upper Penninic zone (Trümpy, 1980). With the laboratory measurements it is possible to investigate the influences of seismic anisotropy and cracks that affect the velocity of rock types encountered by the seismic survey. Similar studies have been carried out by Fountain (1976, 1986), Burke and Fountain (1990), Barruol and Kern (1996) for the Ivrea–Verbano in the Southern Alps, or by Sellami *et al.* (1990) on the Central Alps on the several lithologies sampled by the NFP-20 East profile. Moreover, the seismic properties of a calcite mylonite from the Alps were determined from the Orientation Distribution Function by Mainprice *et al.* (1990).

The exposed portion of the terranes can serve as a geometrical constraint for the reconstruction of an interpretative seismic model, even though the tectonic complications imposed during uplift have altered the complete cross section. This approach attaches a special importance to structural geology and tries to relate all the observed metamorphism–deformation–seismic relationships to the different regional tectono-metamorphic events described in this part of the upper Penninic nappes (Tambo and Suretta nappes) (see review in Marquer *et al.*, 1994). We make use of the new detailed tectonic framework of the frontal part of the Suretta nappe described by Marquer *et al.* (1996). One of the main results of these recent studies in the Tambo and Suretta nappes is the evidence for a strongly heterogeneous deformation which affected the basement during the Tertiary tectonics, leading to lenses of relatively undeformed domains surrounded by mylonite zones at different scales. Heterogeneous deformation in basement rocks, especially in those with an initially homogeneous and isotropic structure (e.g. granites), is often expressed by anastomosing shear zones surrounding lenses of weakly deformed rocks (e.g. Mitra, 1978, 1979; Ramsay and Allison, 1979; Bell, 1981; Choukroune and Gapais, 1983; Marquer, 1991). This peculiar geometry associated with heterogeneous deformation favours a precise deformation–metamorphism analysis along strain gradients, such as mylonite zones.

Via the famous example of the Tambo and Suretta nappe piles located in the central Alps, this paper examines in detail the relationships between the crystallographic fabric and the seismic properties (anisotropy) of the marbles lying between the two nappes and which are the likely source of the reflectors seen in the *in situ* seismic profiles.

GEOLOGICAL SETTING

The central Swiss Alps can be divided into the three following domains (Fig. 2a): (i) an external part, the Helvetics, (ii) an internal part, the Pennine zone, and (iii) the South-Alpine units (Coward and Dietrich, 1989). The Penninic zone consists of imbricate stacks of sedimentary cover and basement slices and results from the collision between the European plate in the north and the Adriatic

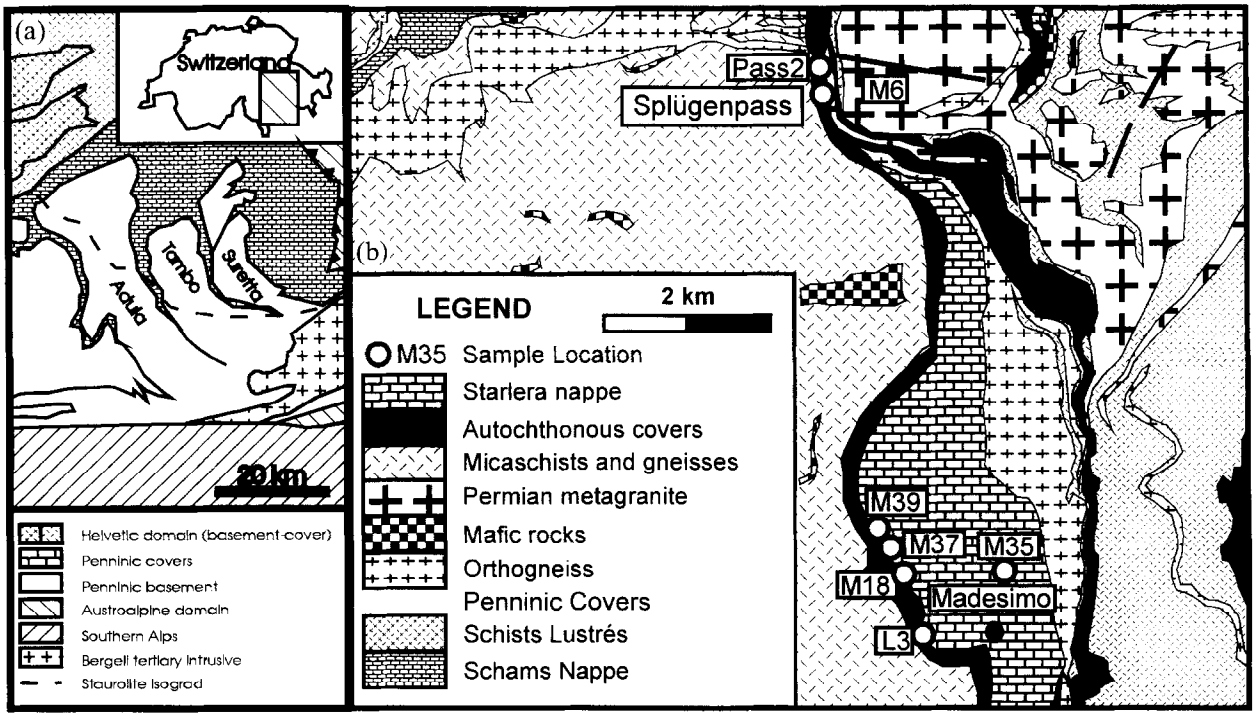

Fig. 2. (a) Location of the study area on a sketch map of the eastern Alps, is marked by a black square on the inset. (b) Geological map of the middle part of the Suretta and Tambo nappes and sample localities. Original geological survey of the Suretta and Tambo nappes by D. Marquer.

plate in the south. New metamorphic and structural investigations carried out in the Suretta, Tambo and Adula nappes (Heinrich, 1982; Low, 1987; Baudin *et al.*, 1993; Marquer *et al.*, 1996) taking advantage of new geophysical data and reflection seismic profiles from the National Research Program NFP-20 on the deep structure of Switzerland (Schmid *et al.*, 1990; Pfiffner *et al.*, 1988, 1990a,b) described the nappe geometry in terms of thrust tectonics and post-nappe refolding.

The Tambo and Suretta nappes form thin crystalline slivers, each about 3.5 km thick, essentially composed of metapelites and metagreywackes, including some lenses of mafic rocks (amphibolites) and local migmatites, and are intruded by pre-Alpine magmatic bodies, such as old porphyritic orthogneisses and lower Permian subvolcanic intrusions. The nappes are covered by autochthonous sedimentary cover composed of an old crystalline basement and small occurrences of Permian rocks. This cover is called 'Permo-Triassic' (Staub, 1958). The nappes are separated by different Mesozoic covers which show important thickness variations: (i) the Misox zone, between the Tambo and Adula nappes and (ii) the Splügen zone, between the Tambo and Suretta nappes (Fig. 2). A more detailed description is in Huber and Marquer (1996). Here we briefly introduce the Splügen zone. The autochthonous cover of the Splügen zone varies from a few metres up to several hundred metres in thickness, mainly due to basin formation and Tertiary deformation, and is overlain by a more complete allochthonous cover, the Starlera nappe, according to the latest work of Baudin *et al.* (1995). This thrust slice, always in a normal stratigraphical position, consists from bottom to top of Triassic banded marbles and dolomites, dark malodorous marbles, massive white marbles, calcschists and polygenetic breccias, typical of the internal Briançonnais. It must be pointed out that the 'Permo-Triassic' and the carbonate series of the autochthonous cover are frequently separated from the allochthonous cover by a cargneule layer which evolves from middle Triassic dolomites (and evaporites) belonging to the bottom of the Starlera nappe. Since the cover rocks of the Splügen zone show large variations of thickness and deformation, they were chosen as a representative area for the selection of the marbles.

SAMPLE LOCALITIES AND DESCRIPTION

For the present work, six samples of marble and one of cargneule were selected for the seismic measurements (Table 1). All of these were collected between the Splügenpass and Campodolcino (N Italy, prov. Sondrio). The sample locations are shown in Fig. 2.

Microstructure and shape preferred orientation

Double polished ultrathin sections (5 microns) parallel and normal to the lineation (and normal to the foliation) were prepared for the microstructural analysis, for the determination of the shape preferred orientation (SPO) and for the crystallographic preferred orientation (CPO). A portion of each thin section was digitised from photomicrographs, in order to cover an area containing from 500 to 1000 grains. These were used to determine the modal composition, and to define the SPO. The photomicrographs of the analysed samples, as well as the average dimensions of the grains, are shown in Fig. 3.

Marbles M18, M6 and M39 are dark grey in colour, well banded and foliated, with the banding parallel to the foliation. The banding is defined by alternating darker and lighter bands richer in organic material (malodorous) or in white calcite and yellow dolomite. The foliation trace is defined by the elongation of calcite and dolomite grains. Among these samples, marble M39 shows a strong mineral lineation. Mean grain size ranges between 90 and 110 microns and square-root grain size distributions follow a typical Gaussian distribution (unimodal). Grain boundaries (GB) are generally straight and often show triple junctions. Shape fabric is more intense in marble M6 and lower in M39 (see the ellipses of Fig. 3a). Some of the grains have high temperature twins (type 3 and 4 of Burkhard, 1993), with lensoid shape (indicating twin boundary migration) or are interrupted. A few thin twins probably formed during late deformation which occurred at lower temperature. The temperature obtained with the calcite–dolomite geothermometer (D'Onofrio, 1996, Diploma thesis) ranges between 244 ± 80 and 387 ± 23°C, in agreement with the temperature predicted by Burkhard (1993) from the twin shape, and by E. H. Rutter (personal communication, 1997) on

Table 1. Sample description. The elevation (q) of the sample locality is in m. The modal composition is expressed in percent of calcite (Cc), dolomite (Do), white mica (Mu), quartz (Qz). In all cases opaques and other phases are present at the level of 1% or less. The composition of L_3 is estimated, but the others were measured using an image analysis technique

Sample	Locality	Nappe	Lithology	Modal Composition			
				Cc	Do	Mu	Qz
M6	Splugenpass q.2140	Starlera	Grey marble	**99**			
M18	Pianozzo q.1580	Starlera	Grey marble	**94**	5		
M35	Andossi	Starlera	White marble	**99**			
M37	Teggiate q.1680	Starlera	White marble	**90**	9		
M39	Teggiate q.1690	Starlera	Grey marble	**95**	4		
Pass2	Splugenpass q.2070	Starlera	White marble	**96**	1	1	1
L3	Teggiate q.1650	Starlera–Tambo	Cargneule	**60**	10	10	20

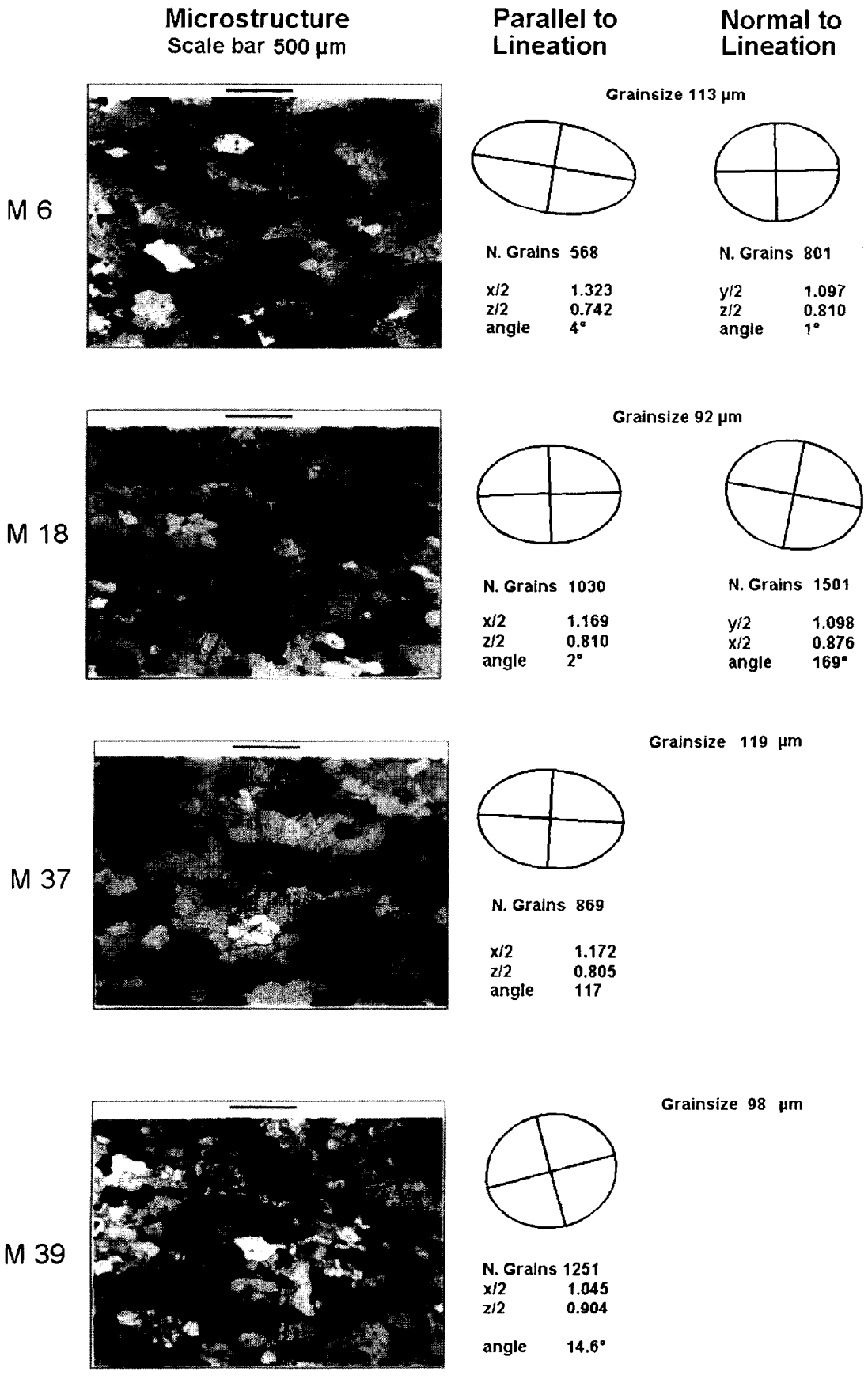

Fig. 3. Shape fabrics: (a) Left side: microphotographs of samples M6, M18, M37 and M39. The long edge of each image is parallel to the trace of foliation and lineation. Right side: grain shape ellipses calculated with the method of Erslev and Ge (1990): parallel (left) and normal (right) to the lineation. The long and short semi-axes are reported and the angle of the long axis with the foliation trace, apparently indicating a sinistral sense of shear (sample M6), a dextral sense of shear for samples M18 and M39. Colour and grain size variations and elongation of clasts define the foliation and lineation of each sample. Grain shapes are generally of similar orientation, but often do not track precisely the mesoscopic fabric elements (see grain shape ellipse sections and orientations). (b) As for (a), but both porphyroclasts and small recrystallised grains are shown. For sample M35 the two directions, parallel and normal to foliation are shown.

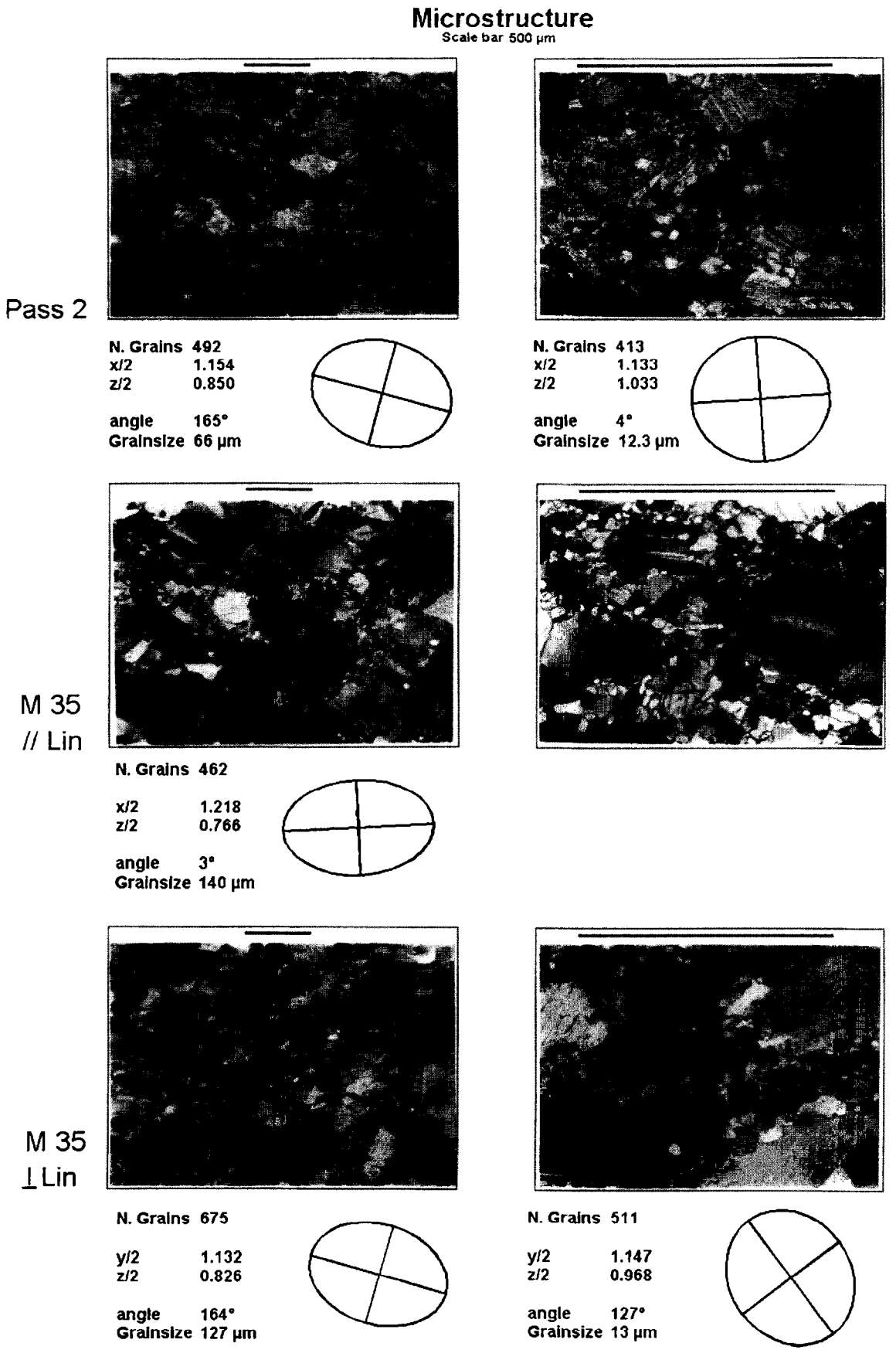
Microstructure
Scale bar 500 µm
Pass 2
N. Grains 492
x/2 1.154
z/2 0.850
angle 165°
Grainsize 66 µm
N. Grains 413
x/2 1.133
z/2 1.033
angle 4°
Grainsize 12.3 µm
M 35
// Lin
N. Grains 462
x/2 1.218
z/2 0.766
angle 3°
Grainsize 140 µm
M 35
⊥ Lin
N. Grains 675
y/2 1.132
z/2 0.826
angle 164°
Grainsize 127 µm
N. Grains 511
y/2 1.147
z/2 0.968
angle 127°
Grainsize 13 µm

Fig. 3. (contd).

the basis of microstructural similarities with experimentally deformed samples.

Marble M37 is white coloured with coincident banding and foliation. The banding is defined by alternations rich in calcite (white) and dolomite (yellow). The grain size is around 120 microns, with a good foam texture and slight shape fabric. Twins are generally straight, thick and interrupted (type 4 of Burkhard, 1993). Among the analysed samples this was equilibrated at the highest temperature (387 ± 22°C) and did not undergo any retrogression.

The final two marbles, M35 and Pass2 are both white in colour, with faint banding and well developed foliation, which are coincident in sample Pass2 and 20° apart in sample M35. The grain size distribution is bimodal. Equant, newly formed strain free small grains rim larger twinned porphyroclasts with undulose extinction. These small grains are about 12–13 microns size in those samples. The porphyroclasts are of 60–70 microns in sample Pass2 and about 130 microns in marble M35. The larger porphyroclasts show a strong shape fabric, and thick lens-shaped twins, indicating twin boundary migration. The small grains develop along the grain boundaries of the porphyroclasts, with a foam texture, and are progressively disoriented with increasing distance from the host grain, indicating rotation recrystallisation. It is therefore inferred that after the twin activity (intracrystalline plasticity) the deformation was accommodated by diffusion creep and dynamic rotation recrystallisation. Using the paleostress relations proposed by Rowe and Rutter (1990), we calculated a peak differential stress of about 80 MPa for both, at a temperature of the order of 300°C (278 ± 30°C for sample Pass2, D'Onofrio, 1996, Diploma thesis).

Crystallographic preferred orientation

The crystallographic fabric was measured optically using a four axis Universal Stage. For each grain, the *c*-axis and the *e*-twin or *r*-plane was measured. The results are reported in Fig. 4 as stereoprojections for the *c*-axis and *e*-twins, and as Inverse Pole Figures (IPF), inverted for the direction of the pole to foliation and for the lineation. It is important to note that the fabric was measured on two orthogonal thin sections for samples M6, M18, M35, M37 and M39, and only on one thin section for sample Pass2. Therefore, all the pole figure maxima of density of the latter sample are much higher than for the others, because some orientations cannot be accounted for in one thin section alone.

The *c*-axis distribution is very similar for all the samples, with a maximum density ranging between 4 and 5 times uniform (note that the maximum density in sample Pass2 is $\times 10.5$ uniform, anomalously high by comparison with the others), oriented approximately parallel to the pole of the foliation. Slight deviation of the *c*-axis concentration from the foliation-normal towards the lineation (monoclinic internal symmetry) as observed in some samples, may be interpretable as due to shearing (e.g. Schmid *et al.*, 1987). Most of these samples have only a slight tendency to monoclinic internal symmetry, implying a sinistral sense of movement on samples M6, M35 and Pass2, and dextral on the others. The small recrystallised grains of samples M35 and Pass2 have a stronger apparent fabric (a smaller number of number of measurements, however), with a monoclinic tendency, implying a dextral (Pass2) and sinistral (M35) movement, respectively. Note the change in the sense of displacement of the maximum of the *c*-axes of sample Pass2 from the fabric of the porphyroclasts to that of the small recrystallised grains.

Twins are generally well oriented, with a density maximum ranging between 4 and 6 times uniform (remember that the maximum of sample Pass2 is anomalously high). Two maxima are present in samples M18, M37 and Pass2, whilst in the others, the poles to twins are more dispersed. The twin poles are roughly oriented parallel to the foliation normal. From the deflection of the two maxima from the foliation normal, it is possible to define a sense of movement, which is dextral for samples M37, M18 and M39, sinistral for sample Pass2, indeterminate in the remainder. This is in agreement with the sense of movement inferred from the *c*-axis fabric.

These fabric types are quite common in naturally deformed marbles at temperature of 250–350°C (compatible with the temperature range estimated using the calcite–dolomite geothermometer) and correspond also to experimentally deformed calcite aggregates in the range of temperature from 600 to 750°C and high strain rate (Casey *et al.*, 1998 this issue), when *r* and *f* glide is easier than the twinning. The rocks therefore acquired this fabric when twin activity was being replaced by *r* and *f* glide. In order better to constrain the possibility that the fabric is caused by *r* and *f* glide, the IPFs for the pole to foliation and lineation were plotted (Fig. 4). On the IPFs of the pole to foliation, the maximum density ranges between 2.7 and 3.3 times uniform. The maximum is parallel to *e* (M39, Pass2), between *e* and *r* (M35 and M18) or with a well defined *r* maximum (with or without *e* max) in samples M37 and M6. Note that sample M6 does not have many thick twins preserved. On the IPFs of the lineation is developed a single maximum density between *f* and *r* (or *h*) (M6 and M35), and a minor

Fig. 4. Crystallographic fabrics: Lower hemisphere equal area projections of the calcite *c*-axis and *e*-twin and Inverse Pole Figure (IPF) (inverted for the pole to the foliation and for the lineation). Contours, in Multiples of Uniform Distribution (m.u.d.), are reported next to each figure. For the pole figure, the normal to the foliation is horizontal E–W and the lineation is horizontal N–S. The N–S line represent the foliation plane and lineation. The maximum density is indicated by a filled black square. For samples M35 and Pass2 also are plotted the *c*-axes of the small recrystallised grains.

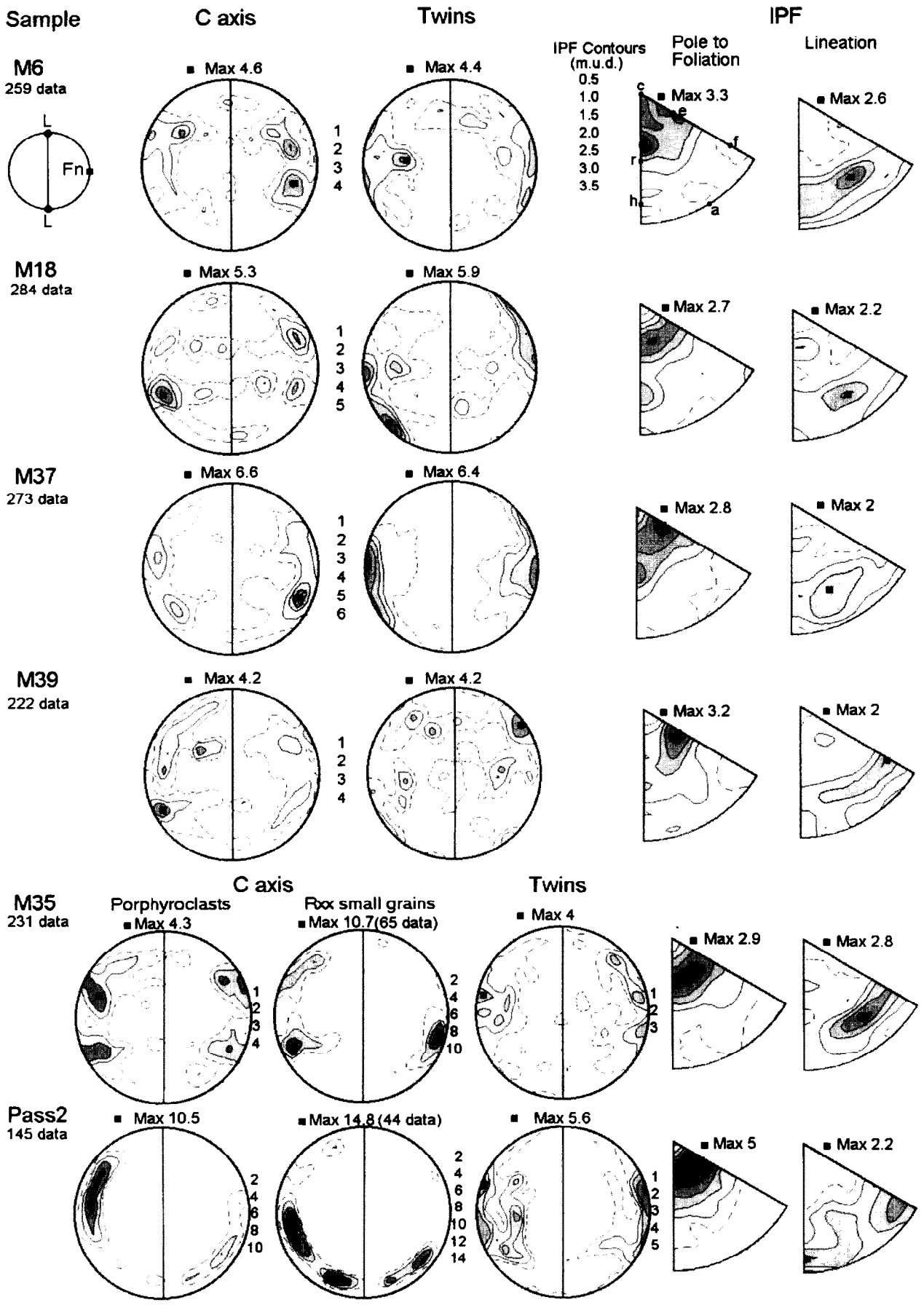
Sample
C axis
Twins
IPF
IPF Contours (m.u.d.)
0.5
1.0
1.5
2.0
2.5
3.0
3.5
Pole to Foliation
Lineation
M6
259 data
L
Fn
L
Max 4.6
Max 4.4
Max 3.3
Max 2.6
M18
284 data
Max 5.3
Max 5.9
Max 2.7
Max 2.2
M37
273 data
Max 6.6
Max 6.4
Max 2.8
Max 2
M39
222 data
Max 4.2
Max 4.2
Max 3.2
Max 2
C axis
Twins
M35
231 data
Porphyroclasts
Max 4.3
Pxx small grains
Max 10.7(65 data)
Max 4
Max 2.9
Max 2.8
Pass2
145 data
Max 10.5
Max 14.8(44 data)
Max 5.6
Max 5
Max 2.2

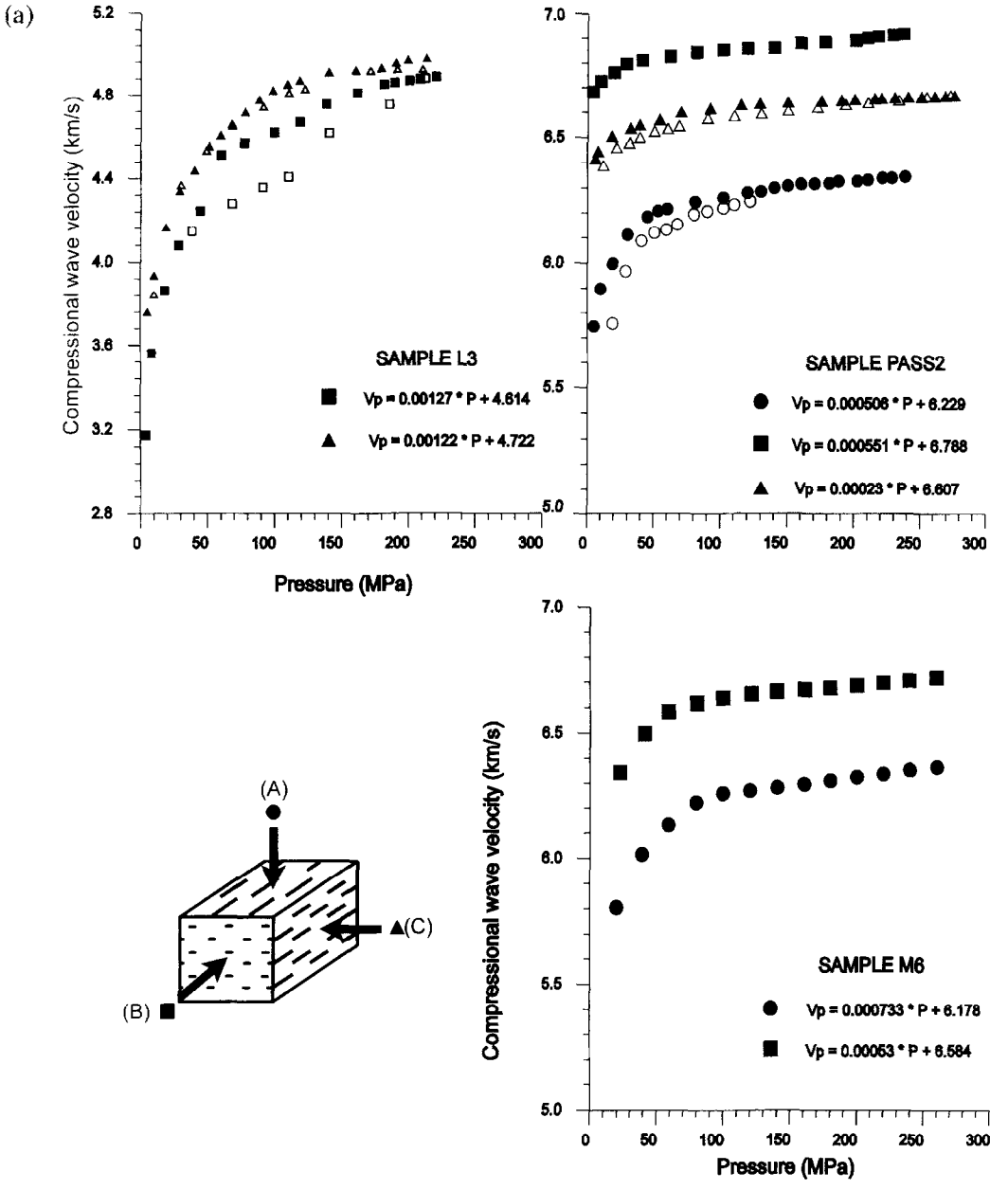

Fig. 5. Confining pressure (in MPa) vs velocity (in km/s) of samples Pass2, M6 and L3 (a) and of samples M18, M35, M37 and M39 (b). The open symbols represent the measurements up-pressure and the filled symbols the measurements down-pressure. Circles are the velocities measured in the direction normal to foliation, squares in the direction parallel to lineation and triangles in the direction normal to lineation and parallel to foliation, as explained in the sketch in the lower left corner. Diamonds of sample M35 refer to the direction at 45° to the lineation in the foliation plane. Below the curves of each sample are reported the linear equation fitting the points at pressures greater than 100–150 MPa, when the curve becomes linear. The constant of the equation is therefore the zero pressure velocity and the slope the velocity derivative with pressure.

concentration towards *a* and *h* (M39, M18 and Pass2) with the exception of sample M37.

Finally, the fabric and microstructure of the small recrystallised grains of samples Pass2 and M35 suggests that a change in deformation mechanism from intracrystalline plasticity into grain-size sensitive flow occurred.

THE EXPERIMENTAL METHOD

The velocity of compressional elastic waves in the marble rock samples were measured at confining pressures of up to 300 MPa at the Laboratory of Petrophysics of Milano (Italy) using the pulse transmission technique (Birch, 1960).

In order to determine the directional dependence of the seismic wave velocities, three mutually perpendicular cylinders (26 mm in diameter and 35–55 mm in length) were cored from each sample, parallel and perpendicular to the external fabric elements of the rock (foliation and lineation). In this paper we follow the convention that the **A** core is normal to the foliation, the **B** core is parallel to the mineral lineation and the **C** core is normal to the lineation and parallel to the foliation (see inset of Fig. 5a).

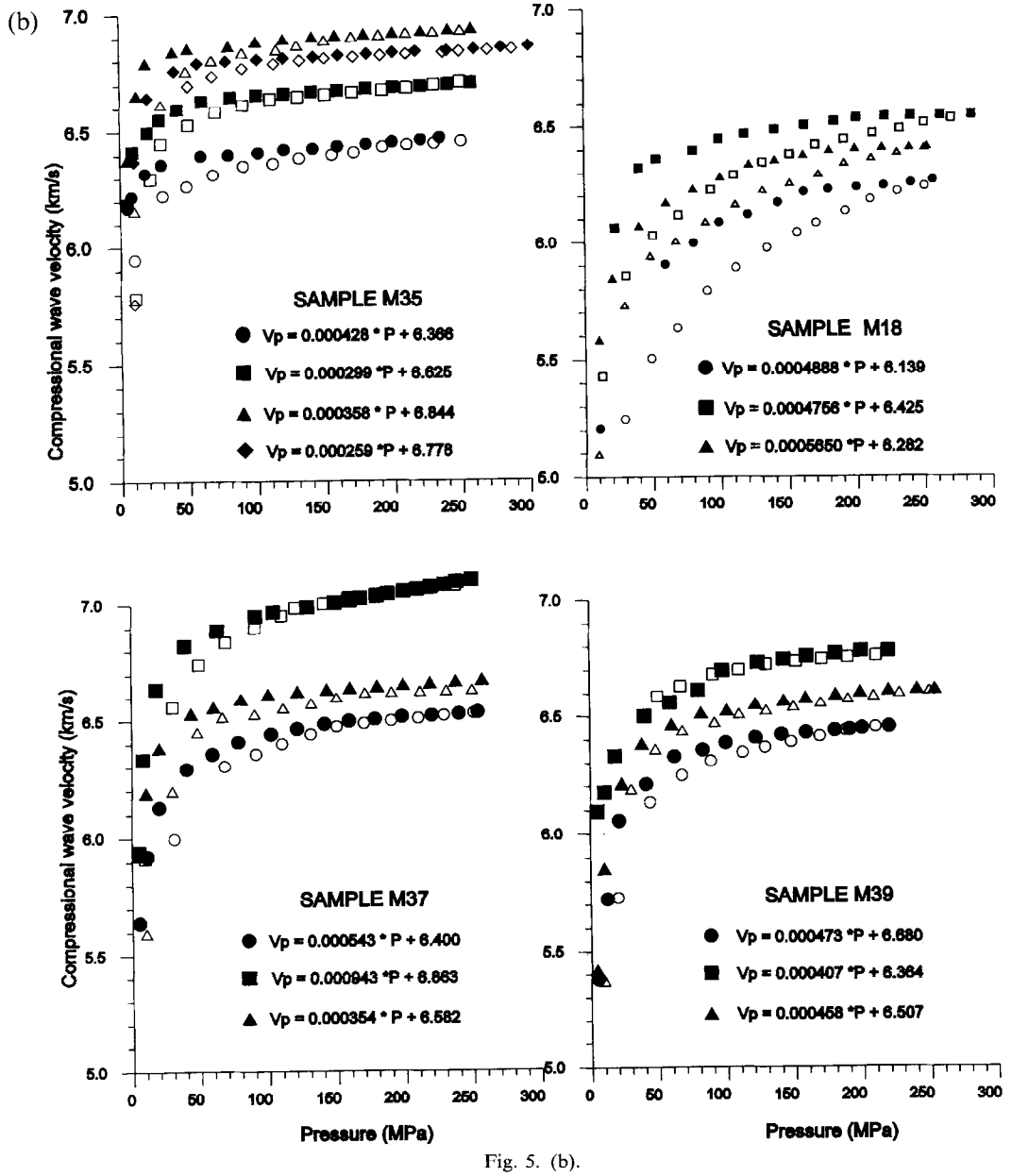

Fig. 5. (b).

For the sample M6, only the directions parallel to the lineation and normal to the foliation were cut, whilst for sample M35 another direction, parallel to the foliation and at 45° to the lineation, was cored, in order better to constrain the overall seismic properties.

The core ends were ground parallel within ± 0.02 mm, and were oven dried for at least 12 hr, at a temperature of 80°C. Core dimensions were measured ± 0.005 mm, and weighed to within ± 0.0001 g. Bulk density was determined from dimensions and weights. On both ends of the core specimen a brass foil of 0.2 mm thickness ensured electrical continuity between the transducers and the common pole. The piezoelectric transducers, placed next to the brass foils, were silver plated piezoelectric ceramics (lead zirconate) with a resonant frequency of 1 MHz. The specimen was wrapped with Teflon and plastic tape and jacketed with 3 mm thick PVC tubing in order to ensure isolation from the oil. The pressure vessel can reach 300 MPa, which is generally enough to close most of the microcracks and pore spaces in calcite rocks. The pressure at 300 MPa was measured to ± 1 MPa.

The electronic system consists of a pulse generator and a waveform analyser. Both are PC-IBM compatible plug-in 8-bit cards. The pulse generator card produces a square wave of up to 300 V amplitude with a rise of less than 10 ns into 50 ohm with a repetition rate variable from 0.2 to 2 ms in one microsecond steps. The 100 MHz–800 MHz (in equivalent time sampling) waveform analyser has a RAM of 128 kbyte. Typically 6400 waveforms of 1200 points each were averaged for each measurement, recording a 12 μs duration seismogram. The precision of the time measurement is within ± 0.01 μs. The cables, the PC plug-in cards, the transducers and the brass foils introduce delays on the order of 0.16 ns in the observed travel time.

EXPERIMENTAL RESULTS

The elastic wave velocities were measured at increasing confining pressures at 20 MPa increments until the maximum pressure was reached, then at decreasing confining pressure separated by 20 MPa decrements. Because the velocities varied rapidly at low confining pressures, the measurements were carried out also at 10 and 5 MPa. The confining pressure/velocity relations are reported in Fig. 5. The non-linear parts of the curves are generally interpreted as due to crack and pore closure (Birch, 1961), whilst the linear parts (at high pressure) reflect the intrinsic seismic properties of the rocks: i.e. the crack-free matrix properties. The matrix seismic properties correspond therefore to the maximum velocities possible for the rock type under consideration. All the other factors, such as temperature and pore pressure, can only reduce the seismic velocities if no chemical reactions or polymorphic transformations take place (Walsh, 1973).

The velocity measured during pressurisation is always lower than that measured during depressurisation, suggesting that some of the cracks or pore spaces do not reopen during depressurisation (hysteresis). The hysteresis was more pronounced in the cargneule than in the marbles and, among the marbles, in samples M35 and M18. According to Burke (1987), measurements made during pressurisation are not reproducible, whilst those during depressurisation are reproducible.

From the graphs shown in Fig. 5 it is evident that most of these marbles reach the linear part of the velocity/pressure relation at relatively low pressure (100 MPa) compared to silicate rocks, indicating that cracks and pore spaces close rapidly, whilst the cargneule reaches the linear part only at the highest pressures. In the latter case, the pressure derivatives, calculated from the linear part of the velocity/pressure curve at pressures greater than 100–150 MPa, are probably too high, even though, as in this specific case, they were determined at pressures greater than 150 MPa.

Regarding the marble samples, the minimum velocity (6.3–6.6 km/s @ 250 MPa confining pressure) is always for propagation direction normal to the foliation (A cores), the maximum (6.5–7.1 km/s @ 250 MPa) is for propagation parallel to the lineation (B cores), and intermediate for propagation parallel to the foliation and normal to the lineation (C cores). An exception to this generalisation is given by sample M35 where the maximum velocity was found to be normal to the lineation and the intermediate parallel to the lineation (both within the foliation plane). For this reason another core was cut in an intermediate direction. The cargneule is instead almost isotropic at high pressure and has a very low seismic velocity (4.9 km/s @ 200 MPa confining pressure).

The elastic wave velocities measured at the maximum pressure, their pressure derivatives calculated from the linear portion of the velocity/pressure relation, the intrinsic zero pressure intercept velocities calculated using the pressure derivatives, the densities and the acoustic impedances are listed in Table 2 for each sample and each propagation direction. In Table 2, for each sample are also listed the mean velocity, the anisotropy and the four parameters (a, A, b, B) suggested by Wepfer and Christensen (1991) to fit the experimental measurements into an empirical formula of the form:

$$V_p(P) = A(P/100)^a + B(1 - e^{-bP}) \quad (1)$$

where V_p is the velocity in km/s and P is the confining pressure in MPa.

The dependence of the wave velocity with direction is direct evidence of seismic anisotropy. Here the intrinsic seismic anisotropy (A) is defined as follows:

$$A\% = 200(V_{p\max} - V_{p\min})/(V_{p\max} + V_{p\min}). \quad (2)$$

The intrinsic anisotropy of the marbles ranges between 4.2 and 8.6% at the maximum pressure. The anisotropy vs confining pressure (Fig. 6) generally decreases with pressure, indicating that the cracks contribute to the total anisotropy in a constructive manner because they are probably mainly oriented parallel to the foliation. In other words, at low pressure, or when pore pressure keeps open the cracks, we should expect a higher anisotropy. Samples M18, M37 and M39 do not follow this generalisation, suggesting that intrinsic properties and cracks interfere in a destructive manner, or that crack families, oriented in different way, close selectively at different confining pressures.

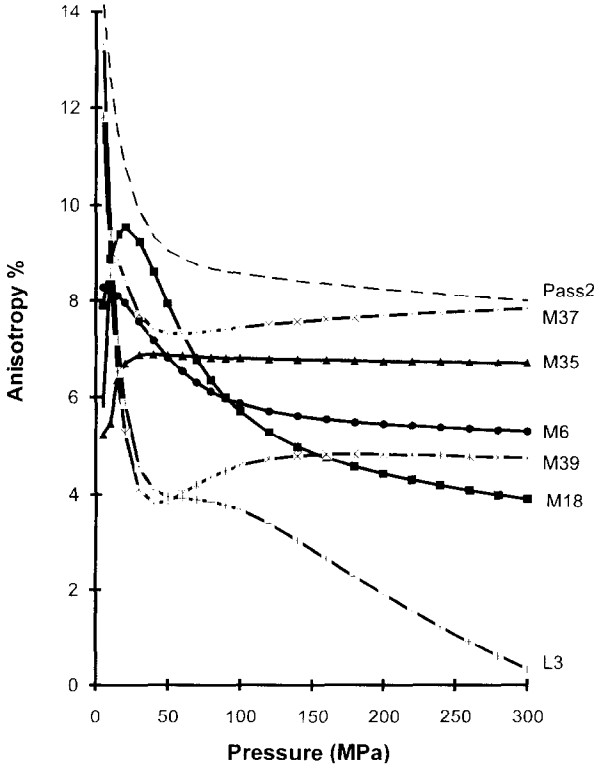

Fig. 6. Seismic anisotropy (%) vs confining pressure (in MPa) diagram for all the samples.

Table 2. Seismic properties of the samples described in Table 1. The elastic wave velocities measured at 250 MPa confining pressure and the calculated zero-pressure velocity from the V_p derivatives are listed into the first two columns; in the third column are listed the pressure derivatives calculated from the linear portion of the velocity/pressure relation and in the fourth column, the densities. The acoustic impedances calculated for the velocities measured at 250 MPa and zero-pressure are listed, respectively, in the fifth and sixth columns. In the last five columns are listed the four parameters suggested by Wepfer and Christensen (1991) to fit the experimental measurements into the empirical formula $V_p(P) = A(P/100)^a + B(1 - e^{-bP})$ and the maximum discrepancies between the calculated and experimental values. For each sample the letters **A**, **B** and **C** refer to the propagation direction (see text)

Sample	V_p250	V_p0	dV/dP	dens	Z250	Z0	**A**	**a**	**B**	**b**	Maximum error
Pass2A	6.35	6.23	$5.06 \times 10-4$	2.70	17.14	16.81	5.91	0.015	0.361	0.079	0.0195
Pass2B	6.91	6.79	$5.51 \times 10-4$	2.70	18.64	18.30	6.81	0.006	0.072	0.013	0.0185
Pass2C	6.67	6.61	$2.30 \times 10-4$	2.70	17.97	17.81	6.53	0.009	0.082	0.199	0.0110
Mean	6.64	6.54	$4.29 \times 10-4$	2.70	17.91	17.64					
Anis (%)	8.46	8.59									
M18A	6.28	6.14	$4.89 \times 10-4$	2.70	16.96	16.59	5.37	0.033	0.744	0.039	0.0258
M18B	6.55	6.43	$4.76 \times 10-4$	2.69	17.60	17.27	5.40	0.019	1.054	0.082	0.0334
M18C	6.43	6.28	$5.65 \times 10-4$	2.69	17.28	16.88	5.68	0.026	0.617	0.059	0.0195
Mean	6.42	6.28	$5.10 \times 10-4$	2.69	17.28	16.91					
Anis (%)	4.22	4.55									
M35A	6.46	6.37	$4.28 \times 10-4$	2.70	17.44	17.19	6.21	0.008	0.201	0.163	0.0113
M35B	6.70	6.63	$2.99 \times 10-4$	2.69	18.00	17.79	5.37	0.013	1.275	0.393	0.0315
M35C	6.93	6.84	$3.58 \times 10-4$	2.67	18.49	18.27	6.05	0.007	0.834	0.194	0.0213
M35D	6.84	6.78	$2.59 \times 10-4$				5.60	0.007	1.204	0.151	0.0077
Mean	6.73	6.65	$3.36 \times 10-4$	2.69	17.98	17.75					
Anis (%)	6.96	7.24									
M37A	6.54	6.40	$5.43 \times 10-4$	2.67	17.49	17.11	5.73	0.021	0.704	0.108	0.0144
M37B	7.09	6.86	$9.43 \times 10-4$	2.68	19.00	18.39	5.00	0.031	1.951	0.294	0.0321
M37C	6.67	6.58	$3.54 \times 10-4$	2.71	18.09	17.85	5.95	0.012	0.652	0.112	0.0084
Mean	6.77	6.62	$6.13 \times 10-4$	2.69	18.19	17.78					
Anis (%)	8.08	6.98									
M39A	6.47	6.68	$4.73 \times 10-4$	2.67	17.27	17.84	5.32	0.018	1.064	0.09	0.0412
M39B	6.79	6.36	$4.07 \times 10-4$	2.66	18.09	16.95	6.28	0.013	0.441	0.031	0.0310
M39C	6.62	6.51	$4.58 \times 10-4$	2.69	17.78	17.48	5.41	0.018	1.119	0.103	0.0222
Mean	6.62	6.52	$4.46 \times 10-4$	2.67	17.71	17.43					
Anis (%)	4.90	4.85									
M6A	6.35	6.18	$7.33 \times 10-4$				5.60	0.017	0.659	0.046	0.0130
M6B	6.71	6.58	$5.30 \times 10-4$				6.00	0.013	0.639	0.066	0.0080
Mean	6.53	6.38	$6.32 \times 10-4$								
Anis (%)	5.51	6.36									
L3B	4.96	4.61	$1.27 \times 10-3$	2.29	11.33	10.54	3.99	0.085	0.643	0.071	0.0964
L3C	5.01	4.72	$1.22 \times 10-3$	2.32	11.64	10.97	4.11	0.038	0.754	0.031	0.0243
Mean	4.98	4.67	$1.25 \times 10-3$	2.30	11.48	10.76					
Anis (%)	1.07	2.31									

Most of the marble samples display an orthorhombic symmetry of the compressional wave velocity. In fact, the velocity in the **C**-core direction of sample M39, M18 and Pass2 is almost exactly equal to the mean between the velocities measured in the **A** and **B** directions. As previously described, the situation for sample M35 is opposite (**B** and **C** maxima reversed), but the orthorhombic symmetry is still maintained. Quite different is the anisotropy of sample M37, where the velocity normal to the foliation (**A**-core) and normal to lineation, parallel to foliation (**C**-core) are very close to each other and much lower than that parallel to the lineation (**B**-core). We could define this as a transverse isotropy with the axis of rotational symmetry parallel to the mineral lineation.

Because of these peculiarities of the measured seismic properties, and because of the assumption that the reference frame of the rock (foliation and lineation) coincides with the principal axes of the seismic properties, we decided to calculate the seismic properties in any direction adopting the well established method of Mainprice (1990), using the CPO and the single crystal elastic constants of Dandekar (1968). The results will be described in the next paragraph.

The averaged velocities, as well as those propagating in the direction normal to the foliation, were used to calculate the acoustic impedance and the vertical reflectivity for the isotropic and anisotropic case, respectively, for the marbles and for all the lithologies in contact with the marbles (quartzites, gneisses, schists, amphibolites) in the same manner as described by Khazanehdari *et al.* (1998) (this issue). For the other lithologies we used the velocities and densities reported in Carmichael (1989). The reflection coefficients are reported in Table 3. The reflection coefficients greater than 0.04 (bold number in Table 3) can cause a good reflection observable in a vertical reflection profiling (Sheriff and Geldart, 1995). Therefore, the contact between the cargneule and all the other lithologies, or between marbles and schists or amphibolites are potentially good reflectors.

Table 3. Reflection coefficients. These are the reflection coefficients for normal incidence calculated for contacts between the analysed samples at extrapolated to zero pressure (a) and 250 MPa confining pressure (b) at room temperature for the isotropic case and (c, d) anisotropic case; and the coefficient calculated for the marbles in contact with other lithologies at extrapolated to zero pressure velocity (e) and at 250 MPa confining pressure (f). In bold are the reflection coefficients greater than 0.04: i.e. those producing an observable good reflection in a vertical seismic profile

a) Marbles, room pressure, averaged velocity

sample	M18	M35	M37	M39	M6	L3
Pass2	0.02	−0.01	−0.01	0.00	0.01	**0.17**
M18		−0.03	−0.03	−0.02	−0.01	**0.15**
M35			0.00	0.01	0.02	**0.18**
M37				0.01	0.02	**0.17**
M39					0.01	**0.17**
M6						**0.16**

b) Marbles, 250 MPa, averaged velocity

M18	M35	M37	M39	M6	L3
0.02	−0.01	−0.01	0.00	0.01	**0.14**
	−0.02	−0.03	−0.02	−0.01	**0.13**
		0.00	0.01	0.02	**0.15**
			0.01	0.02	**0.15**
				0.01	**0.14**
					0.13

c) Marbles, anisotropic — room pressure

sample	M18A	M35A	M37A	M39A	M6A	L3A
Pass2A	0.01	−0.01	−0.01	−0.03	0.00	**0.15**
M18A		−0.02	−0.02	**−0.04**	0.00	**0.14**
M35A			0.00	−0.02	0.01	**0.16**
M37A				−0.02	0.02	**0.16**
M39A					**0.04**	**0.18**
M6A						**0.14**

d) Marbles, anisotropic — 250 MPa

M18A	M35A	M37A	M39A	M6A	L3A
0.01	−0.01	−0.01	−0.01	0.00	**0.12**
	−0.01	−0.02	−0.01	−0.01	**0.12**
		- 0.01	0.00	0.01	**0.13**
			0.01	0.01	**0.14**
				0.01	**0.13**
					0.12

Other lithology acoustic impedances

LITHOLOGY	Vp250	Vp0	den	Z250	Z0
Schists	7.20	6.90	2.98	21.46	20.56
Marbles	6.62	6.50	2. 69	17.81	17.48
Cargneule	4.98	4.67	2.3	11.46	10.74
Orthogneisses	6.40	6.20	2.65	16.96	16.43
Quartzites	6.26	6.06	2.77	17.34	16.79
Amphibolites	7.20	7.00	2.85	20.52	19.95

e) room pressure, averaged velocity

LITHOLOGY	Marbles	Cargneules	Orthogneisses	Quartzites	Amphibolites
Schists	**0.08**	**0.31**	**0.11**	**0.10**	0.02
Marbles		**0.24**	0.03	0.02	**−0.07**
Cargneule			**−0.21**	**−0.22**	**−0.30**
Orthogneisses				−0.01	**−0.10**
Quartzites					**−0.09**

f) 250 MPa, averaged velocity

LITHOLOGY	Marbles	Cargneules	Orthogneisses	Quartzites	Amphibolites
Schists	**0.09**	**0.30**	**0.12**	**0.11**	0.02
Marbles		**0.22**	0.02	0.01	**−0.07**
Cargneule			**−0.19**	**−0.20**	**−0.28**
Orthogneisses				−0.01	**−0.09**
Quartzites					**−0.08**

Calculated velocities from CPO

The seismic velocities in all the directions were calculated by the method described by Mainprice (1990), using the computer programs he recently developed. We used the same elastic constants and procedure as in Khazanehdari *et al.* (1998) (this issue), without considering the minor effects due to the presence of dolomite in samples M18, M37, M39 and Pass2 and opaques, because the total amount of calcite in all the samples is always greater than 90% (see Table 1). The calculated V_p, V_s1 (fastest shear wave), shear wave birefringence (V_s1-V_s2) and V_s1 polarizations are shown in Fig. 7. These were calculated for room pressure and temperature using the VRH averaging scheme, because, according to Mainprice and Humbert (1994), it gives the best results for anisotropic rocks. Calculated stiffness tensors for the sample measured are shown in Table 4.

The experimental velocities compare fairly well with the calculated (see Fig. 7). For comparison, the velocities measured at 250 MPa confining pressure are plotted in the stereoprojections of the calculated V_p. We used the velocities at 250 MPa instead of that calculated at zero pressure from the linear fit in order to avoid any effect of errors in the pressure derivatives.

The most important findings are as follows:

a) The slowest V_p is always normal to the foliation; therefore the compressional waves propagate faster parallel to the foliation with a single (M37, M35, Pass2) or two distinct maxima of velocity (M6 and M18) or with a girdle parallel to the foliation (M39). Samples M39, M37, M18 and M6 are characterised by a concentration of *r*-axes (IPFs of Fig. 4). The seismic anisotropy symmetry of those samples is therefore close to transversely isotropic, whilst that of sample Pass2 is orthorhombic. Note that for Pass2 the fabric was determined in one direction alone, and there is a

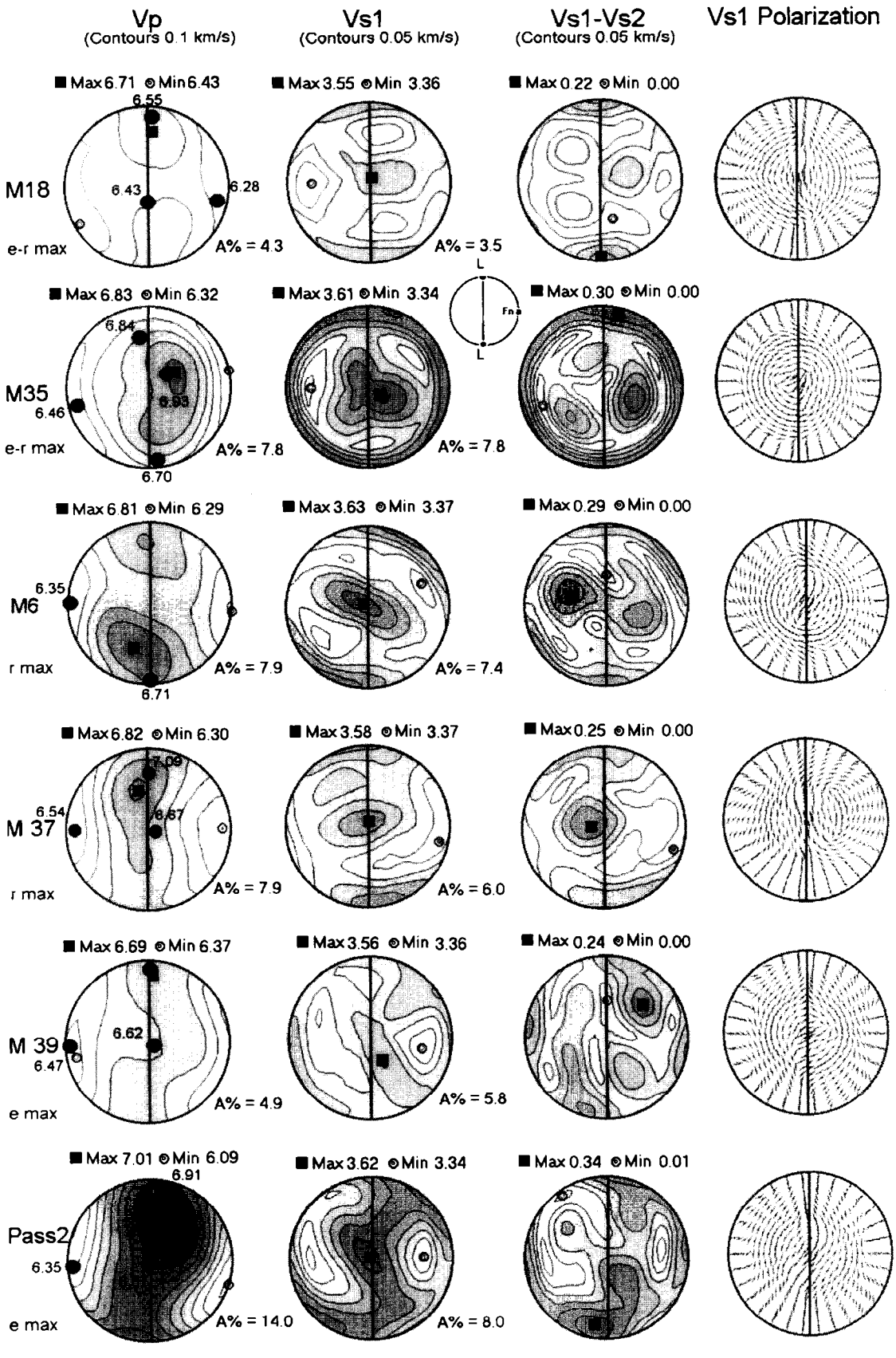

Fig. 7. Equal area stereoprojections of the V_p, V_s1, V_s birefringence and V_s1 polarisations. The lineation is N–S and the pole to foliation is E–W; contours (in km/s). Calculated anisotropy and maximum and minimum velocities are reported near each stereoprojection. Below each sample name is reported the type of fabric.

Table 4. Stiffness tensor of calcite single crystal (Dandekar, 1968) and of the samples calculated using the method outlined by Mainprice (1990). The C_{ij} are in Mbar

	Calcite	M6	M18	M35	M37	M39	Pass2
C11	1.4627	1.2195	1.1940	1.1450	1.1997	1.2086	1.2407
C22	1.4627	1.0797	1.1336	1.0892	1.0808	1.1122	1.0312
C33	0.8531	1.1574	1.1705	1.2145	1.2187	1.1737	1.2597
C44	0.3405	0.3292	0.3193	0.3470	0.3091	0.3375	0.3336
C55	0.3405	0.3498	0.3397	0.3475	0.3459	0.3299	0.3416
C66	0.4328	0.3101	0.3049	0.3001	0.3121	0.2998	0.2901
C12	0.5971	0.5262	0.5197	0.5108	0.5246	0.5139	0.5025
C13	0.5076	0.5745	0.5609	0.5712	0.5742	0.5525	0.5794
C14	−0.2076	0.0062	−0.0120	−0.0144	0.0094	0.0011	−0.0029
C15	0.0000	−0.0051	0.0075	−0.0165	0.0161	0.0034	0.0354
C16	0.0000	0.0079	0.0033	0.0087	−0.0058	−0.0163	−0.0321
C23	0.5076	0.5398	0.5333	0.5643	0.5230	0.5506	0.5500
C24	0.2076	0.0039	0.0054	−0.0039	0.0023	−0.0175	−0.0102
C25	0.0000	−0.0063	−0.0011	0.0007	0.0031	−0.0018	0.0149
C26	0.0000	−0.0081	0.0063	0.0037	−0.0059	0.0084	−0.0274
C34	0.0000	0.0062	−0.0058	−0.0297	0.0228	−0.0069	−0.0287
C35	0.0000	−0.0125	−0.0017	0.0037	0.0025	−0.0030	0.0182
C36	0.0000	−0.0144	0.0027	−0.0025	0.0068	−0.0067	−0.0263
C45	0.0000	−0.0144	0.0016	−0.0036	0.0074	−0.0057	−0.0197
C46	0.0000	−0.0042	−0.0014	0.0016	0.0013	−0.0019	0.0094
C56	−0.2076	0.0047	−0.0108	−0.0096	0.0061	0.0027	0.0017

discrepancy between the observed and calculated velocities. We are therefore sceptical about the results from the calculated velocities. The main differences of the seismic anisotropy structure of samples characterised by an r maximum is a result of the formation of two distinct maxima of V_p parallel to the foliation plane (tetragonal symmetry, with maximum symmetry axis normal to the foliation).

b) The shear waves show very complicated patterns. It is worth noting that there is always a maximum of the V_s1 and shear wave birefringence in a direction almost parallel to the lineation. Again, it is possible to recognise similar patterns in samples with similar CPOs. Two V_s1 maxima are found on samples with an r-max fabric (M37, M6, M18 and M37), one of which is parallel to the mineral lineation and one normal to it, both within the foliation plane. At about 45° to the mineral lineation within the foliation plane, there are two or three minima of V_s1, sometimes reflecting the trigonal symmetry of calcite, with maximum V_s1 symmetry axis normal to the foliation. In the sample with an e-max fabric, the minima are displaced towards the normal to the foliation. The shear wave birefringence has a pattern very similar to that of V_s1.

c) The polarisations of the fastest shear wave show a very complicated pattern.

DISCUSSION AND GEOLOGICAL IMPLICATIONS

In this paper we described the method for the measurements of the elastic wave velocities on naturally deformed calcite rock specimens under high confining pressure. This technique has been used for the determination of the seismic properties of the marbles of cover rocks pinched between the Tambo and Suretta nappes, which belong to the eastern Swiss upper Penninic zone.

All these samples show a pronounced seismic anisotropy ranging from about 4% to 9%. The maximum velocity is generally parallel to the mineral lineation, and the minimum is *always* normal to the foliation. The measured velocities compare fairly well with those calculated from CPO data using the method of Mainprice (1990).

We calculated the normal incidence reflection coefficients for the lithologic contacts exposed. The most reflective contacts are those of the marbles with schist and amphibolites, both for the isotropic approximation and the anisotropic case (propagation direction normal to the foliation). These are the so called intrinsic seismic properties, i.e. those of the crack free matrix. In other words, because the reflection coefficients depend upon the seismic velocity, other properties such as pressure, anisotropy, fluid filled cracks and temperature variations affecting the seismic velocity will change the reflection coefficient of the contacts between rock types. It is well established that temperature and pore pressure reduce the seismic velocities, whilst confining pressure increases the velocities. According to many authors (e.g. Christensen, 1965; Kern, 1990), on a normal thermal gradient the effect of the temperature is balanced by that of the confining pressure, indicating that the velocities will not change significantly with depth for a given rock type. Slightly higher velocity will occur in areas with low thermal gradient (Archean continental crust) and lower in younger crust (such as that of the Alpine Chain) for a given rock type. This figure could be greatly different in the case of elevated pore pressure, which keeps fractures open. In this case, any reduction of the compressional velocities will depend upon the pore pressure, the crack density and crack orientation. As we observed (see the

experimental results), at low pressure, when cracks are still open, the total seismic anisotropy decreases with pressure in some cases and increases in other cases, indicating that cracks are mainly oriented parallel to the foliation in the former case and in a different way in the latter. If the cracks are oriented parallel to the foliation, the velocity in a direction normal to the lineation will be selectively more reduced at low pressure than the velocity in the other directions. The importance of this fact can be seen in Table 3. The only reflection coefficient greater than 0.04 between two marbles is for a propagation direction normal to the foliation at zero pressure. In the case that the fractures are oriented in directions other than parallel to the foliation, the situation will be more complicated, but will be affected by a smaller amount by the seismic anisotropy, and therefore the reflection coefficient calculated for the higher pressure will be appropriate.

We finally observed that the marbles show a rapid closure of the fractures with confining pressure compared to silicate rocks (e.g. Kern, 1990; Fountain, 1986; Christensen, 1965). Thus in the case of low confining pressure or of elevated pore pressure, the seismic velocities of the marbles will be less reduced than those of other silicate rocks. The reflection coefficients reported in Table 3(e) for the contact of marbles with schists and amphibolites will be reduced, but for the contact of marbles with orthogneisses and quartzites they will increase, becoming more reflective. The reflection coefficients will be less pronounced for the propagation direction normal to the foliation at contacts with schists and amphibolites (see Burke, 1987 and Fountain, 1976), because the influence of cracks in these rocks will be greater than for other rock types. Therefore, in case of normal incidence and horizontal foliation a contact of schists or amphibolite with marble could produce a very low reflection, whilst that of marble and orthogneisses could be much more reflective.

In order to discuss the geological implications of this work, we adopted the interpretation reported in fig. 4A of Pfiffner *et al.* (1990a). In Fig. 1 is shown the line drawing of the NFP-20 east seismic profile. All the shaded areas contain prominent reflections that could be generated by interfaces containing carbonate rocks, and the darker shaded area is the reflection interpreted as the Splügen zone. From the structural and geological interpretation of the exposed formations, we might expect that at depth the foliation is almost horizontal, that the marbles are in contact with all the lithologies reported in Table 3(e), and that the lateral continuity of the contacts is quite substantial, with the exception of the cargneule. The cargneule, owing to its very low velocity and density, are very reflective when in contact with other lithologies, but the small and very variable thickness, as well as the poor lateral continuity made this a poor candidate for the reflectivity of the contacts of the basement with the cover. From the results reported in Table 3(e) and (f) and from the considerations reported above, we might conclude that at depths greater that 10 km the contacts between schists and amphibolites will be very reflective in the case of no pore pressure, and less reflective in the case of high pore pressure. The contacts between marbles and orthogneisses or quartzites could be transparent, or barely visible in the case of elevated pore pressure. At shallower depths, the contacts between marbles and all the considered lithologies could be reflective. Finally, in the case of a cargneule body thicker than about 50 m and wider than few hundred metres, we can predict a reflection, because the reflection coefficients with the other lithologies are always greater than 0.2.

Because all of the rock types considered here are strongly anisotropic (between 4 and 9% for the marbles, up to 20% for the schists up to 10% for the orthogneisses and the amphibolites (Fountain, 1976)), and the foliation is mainly horizontal, we must consider that the velocities calculated for wide angle refraction will be up to 10% higher that the velocities for the near vertical reflection.

CONCLUSIONS

We have calculated and measured the seismic properties of highly strained marbles from the Splügenpass, (central Alps), and reached the following conclusions:

a) Measured and calculated velocities compare fairly well, which demonstrates that the seismic properties in these pure marbles are determined by the CPO of calcite. The CPO observed in different samples produced different kinds of variation of seismic velocity with direction. In particular: (i) the *e*-max fabric gives a marked V_p axial symmetry, transverse isotropy, or orthorhombic symmetry, whilst for the shear waves the symmetry is lower (monoclinic); (ii) the *z*-max fabric gives maxima in the V_p and V_s1 distribution, both within the foliation plane, at about 45° to the mineral lineation for V_p and normal to the mineral lineation for V_s1.

b) The calculated reflection coefficients for normal incidence reflection are very high for contacts between marbles and schists and amphibolites, which shows that strong reflections observed in the seismic reflection profile NFP-20 are likely to be caused by the carbonate cover rock layers, whether with or without elevated pore pressure.

c) The velocities calculated from wide-angle reflections are up to 10% higher than that for near-vertical reflection because of the high anisotropy of the rock types.

Acknowledgements—The laboratory was financed with CNR contributions and has been set up with the support of Prof. Boriani and the aid of S. Uggeri, F. Uggeri, R. Holloway and E. Rutter. We thank Prof. G. Pasquaré and Dr A. Zappone for assistance in the sampling and for helpful discussions, Prof. E. Rutter for the correction of the English, the multiple suggestions on the calcite fabric and deformation mechanisms and the constructive discussions, and finally G. Lloyd and an anonymous referee for constructive reviews.

REFERENCES

Barruol, G. and Kern, H. (1996) Seismic anisotropy and shear-wave splitting in lower-crustal and upper-mantle rocks from the Ivrea Zone —Experimental and calculated data. *Physics of the Earth and Planetary Interiors* **95**, 175–194.

Baudin, Th., Marquer, D. and Persoz, F. (1993) Basement-cover relationships in the Tambo nappe (central Alps, Switzerland): geometry, structures and kinematics. *Journal of Structural Geology* **15**, 543–553.

Baudin, Th., Marquer, D., Barfety, J. C., Kerckhove, C. and Persoz, F. (1995) A new stratigraphical interpretation of the mesozoic cover of the Tambo and Suretta nappes: Evidence for early Thin-skinned tectonics. *Compte rendu de l'Académie des Sciences Paris*, Série II, **321**, 401–408.

Bell, T. H. (1981) Foliation development: the contribution, geometry and significance of progressive bulk, inhomogeneous shortening. *Tectonophysics* **75**, 273–296.

Birch, F. (1960) The velocity of compressional waves in rocks to 10 kilobars, Part 1. *Journal of Geophysical Research* **65**, 1083–1102.

Birch, F. (1961) The velocity of compressional waves in rocks to 10 kilobars, Part 2. *Journal Geophysical Research* **66**, 2199–2224.

Burke, M. M. (1987) Compressional wave velocities in rocks from the Ivrea-Verbano and Strona-Ceneri zones, Southern Alps, northern Italy: Implications for models of crustal structure, M.S. thesis, University of Wyoming, Laramie.

Burke, M. M. and Fountain, D. M. (1990) Seismic properties of rocks from an exposure of extended continental crust. New laboratory measurements from the Ivrea zone. *Tectonophysics* **182**, 119–146.

Burkhard, M. (1993) Calcite twins, their geometry, appearance and significance as stress–strain markers and indicators of tectonic regime: a review. *Journal of Structural Geology* **15**, 351–368.

Casey, M., Kunze, K. and Olgaard, D. (1998) Texture and microstructure for Solnhofen limestone deformed to high strains in torsion. *Journal of Structural Geology* **20**, 255–267.

Carmichael, R. S. (1989) *Practical Handbook of Physical Properties of Rocks and Minerals*. CRC press, Boca Raton, Florida.

Choukroune, P. and Gapais, D. (1983) Strain pattern in the Aar granite (central Alps); Orthogneiss developed by bulk inhomogeneous flattening. *Journal of Structural Geology* **5**, 411–418.

Christensen, N. I. (1965) Compressional wave velocities in metamorphic rocks at pressures to 10 kilobars. *Journal of Geophysical Research* **70**, 6147–6164.

Coward, M. and Dieterich, D. (1989) Alpine tectonics—an overview. In *Alpine tectonics*, ed. M. P. Coward, D. Dietrich and R. G. Park. Geological Society Special Publication **45**, 1–29.

Dandekar, D. P. (1968) Pressure dependence of the elastic constants of calcite. *Physical Review* **172**, 873–877.

D'Onofrio, G. (1996). Le Carniole del Passo dello Splüga. Diploma thesis, University of Milan.

Erslev, E. A. and Ge, H. (1990) Least squares center to center and mean object ellipse fabric analysis. *Journal of Structural Geology* **10**, 201–209.

Fountain, D. M. (1976) The Ivrea-Verbano and Strona-Ceneri zones, northern Italy: A cross section of the continental crust-new evidence from seismic velocities. *Tectonophysics* **33**, 145–166.

Fountain, D. M. (1986) Implications of deep crustal evolution for seismic reflection seismology. In *Reflection Seismology: The Continental Crust*, American Geophysical Union, Geodynamic Series 14, ed. M. Barazangi and Brown, pp. 1–7. Washington, D.C.

Heinrich, C. A. (1982) Kyanite-eclogite to amphibolite facies evolution of hydrous mafic and pelitic rocks, Adula nappe, Central Alps. *Contributions in Mineralogy and Petrology* **81**, 30–38.

Huber, R. and Marquer, D. (1996) Tertiary deformations and kinematics of the southern part of the Tambo and Suretta nappes (Val Bregeglia, Eastern Swiss Alps). *Schweiz. Miner. Petrog. Mitt.* **76**, 383–397.

Khazanehdari, J., Rutter, E. H., Casey, M. and Burlini, L. (1998) The role of crystallographic fabric in the generation of seismic anisotropy and reflectivity of high strain zones in calcite rocks. *Journal of Structural Geology* **20**, 293–299.

Kern, H. (1990) Laboratory seismic measurements: an aid in the interpretation of seismic field data. *Terra Nova* **2**, 617–628.

Low, S. (1987) Die tektono-metamorphe Entwicklung der nördlichen Adula-Decke. *Beitrëge zur Geologischen Karte Schweiz* **161**, 84.

Mainprice, D. (1990) A FORTRAN program to calculate seismic anisotropy from the lattice preferred orientation of minerals. *Computers and Geosciences* **16**, 385–393.

Mainprice, D., Casey, M. and Schmid, S. (1990) The seismic properties of Alpine calcite and quartz mylonites determined from the orientation distribution function. ECORS-CROP-NFP20-ALPES special volume. *Bulletin del la Société Géologique de France* **156**, 85–89.

Mainprice, D. and Humbert, M. (1994) Methods of calculating petrophysical properties from lattice preferred orientation data. *Surveys in Geophysics* **15**, 575–592.

Marquer, D. (1991) Structures et cinématique des déformations Alpines dans le granite de Truzzo (Nappe de Tambo: Alpes centrales Suisses). *Eclogae Geologicae Helvetiae* **84/1**, 107–123.

Marquer, D., Baudin, T., Peucat, J. J. and Persoz, F. (1994) Rb–Sr micas ages in the Alpine shear zones of the Truzzo granite: The timing of the Tertiary Alpine P–T-deformations in the Tambo nappe (Central Alps, Switzerland). *Eclogae Geologicae Helvetiae* **87**, 225–240.

Marquer, D., Challandes, N. and Baudin, Th. (1996) Shear zone patterns and strain partitioning at the scale of a Pennine nappe: the Suretta nappe (eastern Swiss Alps). *Journal of Structural Geology* **18**, 753–764.

Mitra, G. (1978) Ductile deformation zones and mylonites; The mechanical processes involved in the deformation of crystalline basement rocks. *American Journal of Science* **278**, 1057–1084.

Mitra, G. (1979) Ductile deformation zones in Blue Ridge basement rocks and estimation of finite strains. *Geological Society of America Bulletin* **90**, 935–951.

Pfiffner, O. A., Frei, W., Finckh, P. and Valasek, P. (1988) Deep seismic reflection profiling in the Swiss Alps: Explosion seismology results for line NFP-20 East. *Geology* **16**, 987–990.

Pfiffner, O. A., Frei, W., Valasek, P., Stauble, M., Levato, L., Dubois, L., Schmid, S. M. and Smithson, S. B. (1990) Crustal shortening in the Alpine orogen: results from deep seismic reflection profiling in the eastern Swiss Alps line NFP 20-east. *Tectonics* **9**, 1327–1355.

Pfiffner, O. A., Klaper, E. M., Mayerat, A. M. and Heitzmann, P. (1990) Structure of the basement-cover contact in the Swiss Alps. *Mémoire del la Société Geologique de Suisse* **1**, 247–262.

Ramsay, J. G. and Allison, I. (1979) Structural analysis of shear zones in an Alpinised Hercynian granite (Maggia Lappen, Pennine zone, central Alps). *Schweiz. Mineral. Petrogr. Mitt.* **59**, 251–279.

Rowe, K. J. and Rutter, E. H. (1990) Paleostress estimation using calcite twinning: experimental calibration and application to nature. *Journal of Structural Geology* **12**, 1–17.

Sellami, S., Barblan, F., Mayerat, A. M., Pfiffner, O. A., Risner, K. and Wagner, J. J. (1990) Compressional wave velocities of samples from NFP-20 East profile. *Societa' Geologica Italiana* **1**, 77–84.

Schmid, S. M., Panozzo, R. and Bauer, S. (1987) Simple shear experiments on calcite rocks: rheology and microfabric. *Journal of Structural Geology* **9**, 747–778.

Schmid, S. M., Rueck, P. and Schreurs, G. (1990) The significance of the Schams nappes for the reconstruction of the paleotectonic and orogenic evolution of the Penninic zone along the NFP-20 East traverse (Grisons, Eastern Switzerland). *Mémoire del la Société Geologique de Suisse* **1**, 263–287.

Sheriff, R. E. and Geldart, L. P. (1995) *Exploration Seismology*. Second edition, Cambridge University Press, pp. 592.

Staub, R. (1958) Tektonische Karte der schamser Decken und ihre Umgebung. *Beitrëge zur Geologischen Karte Schweiz (N.F.)* **103**, 184.

Trümpy, R. (1980) Geology of Switzerland, a guide book. In *Part A: An Outline of the Geology of Switzerland*. Schweiz. geol. Komm., Wepf & co, Basel.

Walsh, J. B. (1973) Wave velocity and attenuation in rocks undergoing polymorphic transformations. *Journal of Geophysical Research* **78**, 1253–1261.

Wepfer, W. W. and Christensen, N. I. (1991) A seismic velocity confining pressure relation, with applications. *International Journal of Rock Mechanics and Mining Sciences & Geomechanics Abstracts* **28**(5), 451–456.